Acta Polytechnica **65**(6):705–711, 2025
https://doi.org/10.14311/AP.2025.65.0705

Published by the Czech Technical University in Prague

INFLUENCE OF MR THERMOMETRY ON PREDICTED TEMPERATURE DURING REGIONAL HYPERTHERMIA TREATMENT

Michael Vydra*, Tomas Drizdal†

Czech Technical University in Prague, Faculty of Biomedical Engineering, Department of Biomedical Technology, nám. Sítná 3105, 272 01 Kladno, Czech Republic

* corresponding author: vydrami1@cvut.cz

† corresponding author: tomas.drizdal@fbmi.cvut.cz

Abstract. Hyperthermia treatment involves heating tissues to 40–44 °C in order to enhance the efficacy of radiotherapy and/or chemotherapy. Temperature increase is usually induced by the constructive interference of several electromagnetic waves radiating from external sources and can be monitored using magnetic resonance (MR) thermometry. This study aimed to predict temperature increases from non-invasive MR thermometry electromagnetic exposure during deep regional hyperthermia treatment. A 1.5 T MR birdcage coil was tuned to produce a homogeneous B_1^+ field and simulated together with the Sigma Eye hyperthermia applicator and three available patient models. Results show that electromagnetic exposure during MR measurements increases temperature by 0.027 °C, which is, in the hyperthermia temperature range, insignificant. In addition, our results show that the predicted B_1^+ field homogeneity was influenced by object size and material properties, especially by the water bolus filling the inner part of the applicator.

Keywords: Deep regional hyperthermia, magnetic resonance, MR thermometry.

1. Introduction

Hyperthermia (HT) is an oncology treatment during which the tumour region is heated to a therapeutic temperatures of 40–44 °C, aiming to significantly increase the efficiency of radiotherapy and/or chemotherapy treatments [1–3]. For deeply seated tumours, a constructive interference of several electromagnetic (EM) sources radiated from individual antenna elements in phased array setup is used for temperature elevation in the target region [4, 5]. The heating efficiency depends on the patient's position within the applicator and applied amplitudes and phases of antennas input signals, which can be obtained using the hyperthermia treatment planning (HTP) [6, 7]. It uses EM field and temperature simulations and optimisations with patient-specific 3D model derived from the CT scan placed in the treatment position within the applicator model [8–10]. HTP allows replacing subjective online steering steps in clinical practice based on personal experiences with objective actions controlled by computer optimisations, which have a potential of unifying the treatment quality among HT centers [11]. Monitoring the temperature distribution throughout the duration of the treatment helps to maximise the temperature target coverage and it is also an important aspect to analyse the applied temperature dose and thus the treatment quality and effect [12].

The temperature in the clinical practise is usually monitored using fibre optic or thermistor probes placed superficially or in an interstitial and/or an intraluminal catheters [13, 14]. Extending the temperature information from these discrete measurement points to the whole treatment region is a challenging task and often not possible. Magnetic resonance (MR) thermometry currently represents the only clinically applied method for non-invasive 3D temperature monitoring during a regional HT treatment [15, 16]. It allows to more precisely control the applied EM energy converted into heat within the target region [17]. Proton resonance frequency (PRF) uses a phenomenon called chemical shift and it is the most commonly used MR thermometry method. This method uses the fact that the shielding of free hydrogen atoms in the B_0 field changes locally as a function of temperature, resulting in phase differences [18]. Both MR imaging and HT treatment use the application of radiofrequency (RF) energy to excite spins, which then undergo absorption and subsequent conversion into thermal energy [19]. However, the temperature increase caused by the RF MR exposure during the regional HT was not yet assessed.

The purpose of this study was to determine predictive temperature increase caused by the application of a non-invasive MR thermometry during the regional hyperthermia treatment. First, we have created and tuned 1.5 T MR birdcage coil operating at 64 MHz to obtain a homogenous B_1^+ field of 6 µT. Then, a deep regional hyperthermia Sigma Eye model operating at 100 MHz was imported along with three different 3D human models into the birdcage coil model. For all these three models, we individually tuned the input power of Sigma Eye applicator model in order to

obtain a maximum temperature of 44 °C within the human models throughout the 90 minute duration of the HT treatment. Then, for a 10 % MRI duty cycle and MRI scan every ten minutes, we evaluated the additional temperature increase caused by the RF exposure of the MR system.

2. Materials and methods

2.1. Birdcage coil modelling

A high-pass MR birdcage coil model at 1.5 T, shown in Figure 1, was created in the Sim4Life (v. 7.2, Zürich MedTech AG, Zürich, Switzerland) EM field simulator. The coil was tuned to a resonant frequency of 64 MHz, i.e. the Larmor frequency of a hydrogen nuclei for static magnetic field strength $B_0 = 1.5$ T. Finite-difference time-domain method (FDTD) was used to calculate the EM field of an empty coil, for which we evaluated the B_0 homogeneity change [20]. A harmonic signal with 120 periods applied to two edge sources placed 90° apart was used to produce a circularly polarised RF field. A RF shield, shown in Figure 1, was placed in the close proximity of the birdcage coil, to suppress the RF field from extending beyond the MR system.

To ensure comparability with the study of Murbach et al. [21], which also focuses on 1.5 T MRI, our objective was to obtain a consistent homogeneous field magnitude of 6.00 µT. Achieving this field intensity resulted in 700 W total input power of the birdcage model, divided into a 350 W for each of the two sources, ensuring the generation of circular polarization. The coil conductive structures were modelled as a perfect electrical conductor (PEC) material. We used a maximum FDTD grid step of 2.5 mm, with 1 mm refinement for the MR coil parts, with Uniaxial Perfectly Matched Layers (UPML) type absorption boundary conditions attached in a distance of 500 mm to the computational domain. A harmonic simulation for 120 periods at 64 MHz for the birdcage coil was computed in around two and a half hours using acceleration at NVIDIA GeForce RTX 2080 graphical processor unit (GPU).

2.2. Regional HT treatment modelling

For the HTP in the pelvic region, we used a model of the Sigma Eye regional applicator (BSD Medical Corp., Utah, USA), which consists, in total, of 12 dipole antenna pairs placed in three rings (each ring has four dipole antennas). We computed harmonic simulation for 20 periods at 100 MHz for each antenna using GPU acceleration [22]. To obtain more realistic temperature predictions, three different 3D patient models were used. The first model was created by segmenting CT scans from The Visible Human Project. The other two models, the Duke model and the Ella models (See Figure 2), were obtained from the Sim4Life Virtual Population database [23, 24].

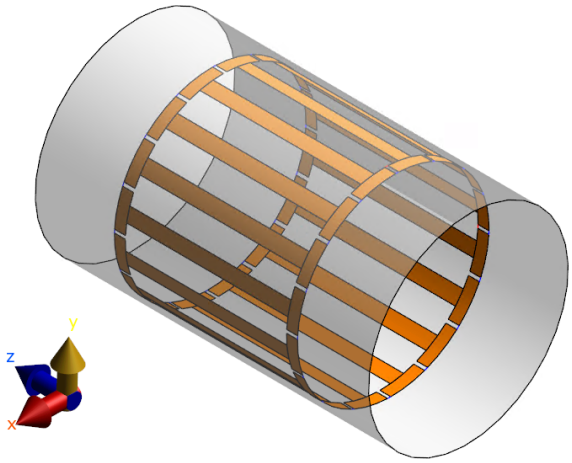

Figure 1. High-pass birdcage MR coil model with the RF shield.

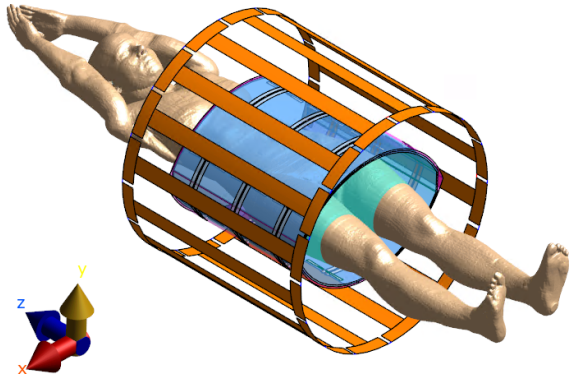

Figure 2. Birdcage coil model with 3D patient model Ella placed in Sigma Eye HT applicator (note that the RF shielding of the MRI is not shown for better visibility of the Ella model).

To investigate the temperature increase due to the RF MR exposure, a 90-minute HT treatment simulation was created to heat the patient up to 44 °C, to which the RF exposure caused by the MR imaging was added. For the HT treatment, we used identical amplitude and phase settings for all antennas and the total power was tuned to obtain the maximum temperature of 44 °C in the human 3D models. For the MR imaging, we used the Gradient Echo sequence where the RF scan was switched on every 10 minutes for a two-second interval calculated using a typical scanning time of 20 seconds and 10 % duty-cycle. The heat generated was distributed throughout the simulated domain by the thermal diffusion and was calculated using the Penne's Bioheat Equation:

$$\rho c \frac{\partial T}{\partial t} = \nabla \cdot (k \nabla T) + \rho Q + \rho S - \rho_b c_b \rho \omega (T - T_b), \quad (1)$$

where ρ [kg m^{-3}] represents the density of the tissue, c [J kg^{-1} K^{-1}] is the specific heat capacity at a constant pressure of the tissue, k [W m^{-1} K^{-1}] is the thermal conductivity, T [K] is the absolute temperature of the tissue, Q [W m^{-3}] is the metabolic heat source, ρ_b [kg m^{-3}] is the blood density, c_b [J kg^{-1} K^{-1}] is

Tissue	ρ [kg m^{-3}]	c [J kg^{-1} K^{-1}]	k [W m^{-1} K^{-1}]
Bones	1 908	1 312	0.320
Bladder	1 086	4 178	0.560
Blood	1 050	3 617	0.516
Brain	1 046	3 630	0.513
Bronchial filling	1.164	10 037*	0.027
Fat	911	2 348	0.212
Gallbladder	1 071	3 716	0.521
Heart muscles	1 080	3 686	0.558
Inner air	1.164	10 037*	0.027
Kidneys	1 066	3 763	0.535
Large intestine	1 088	3 654	0.542
Liver	1 079	3 540	0.519
Lungs	394	3 886	0.387
Muscles	1 090	3 421	0.495
Oesophageal filling	1.164	10 037*	0.027
Small intestine	1 030	3 595	0.493
Spleen	1 089	3 596	0.534
Stomach	1 088	3 690	0.525
Thymus	1 040	3 500	0.527
Trachea filling	1.000	10 040*	0.030

TABLE 1. List of patient model tissues, note that some physical parameters were modified, the specific heat capacity was increased by a factor of 10 to speed up the thermal calculations, which was shown to have no effect on the temperature change [23, 24].

the blood-specific heat capacity at a constant pressure, ω [s^{-1}] is the blood perfusion rate and T_b [K] is the arterial blood temperature. The expression $\rho_b c_b \rho \omega$ is referred to as the heat transfer rate and acts as both heating and cooling, as it represents the blood flow. The maximum difference in median temperature was calculated as follows:

$$\Delta T = (\text{med}.T_{HT+RF} - \text{med}.T_{HT})\,°C, \qquad (2)$$

where med.T is the median of the specified temperature distribution. Since there was a deceleration in the calculation of the temperature simulations due to certain tissue parameters resembling air in density, the specific heat capacity of these tissues has been increased by a factor of 10, see Table 1, which did not influence the accuracy of the temperature predictions.

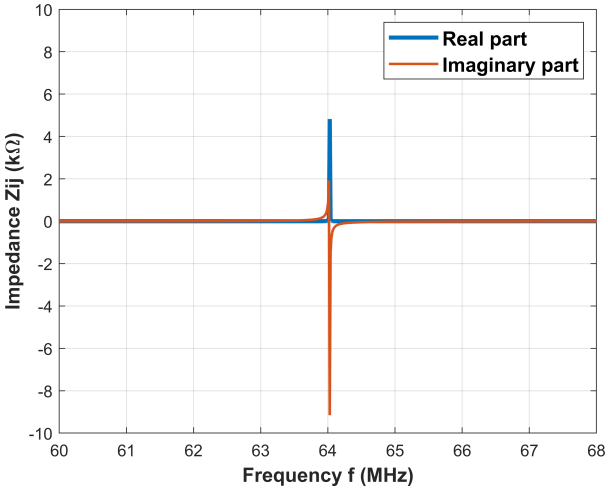

FIGURE 3. Complex impedance curve of a birdcage coil tuned to the resonance frequency of 64 MHz.

3. RESULTS

3.1. BIRDCAGE COIL MODELLING

A complex impedance of an empty birdcage coil, tuned to a resonant frequency of 64 MHz, where imaginary impedance part pass through 0, is shown in Figure 3. After delivering 350 W of power to each source, the coil provides a homogeneous B_1^+ field of (6.00 ± 0.03) µT within a radius of 20 cm from the MR scanner centre. Figure 4a shows an axial cross-section (XY plane from Figure 1 for $Z = 0$ mm). Plot of the B_1^+ field along the X axis in the centre of the MR scanner (green line depicted in Figure 4b) is shown in Figure 4b, from which the B_1^+ field uniformity can be clearly seen.

The presence of the Sigma-Eye applicator (consisting of water bolus, antennas, and shell) increases the B_1^+ field value to (28.51 ± 8.72) µT (see Figure 5). The simulations without the applicator antenna elements do not change these results.

3.2. REGIONAL HT TREATMENT MODELLING

Figure 6a shows an example of the time temperature profile when a total Sigma Eye power of 163 W for Ella model, 205 W for Duke model, and 205 W for 3D model created from CT scan is applied, showing a maximum temperature of 44 °C. Figure 6b

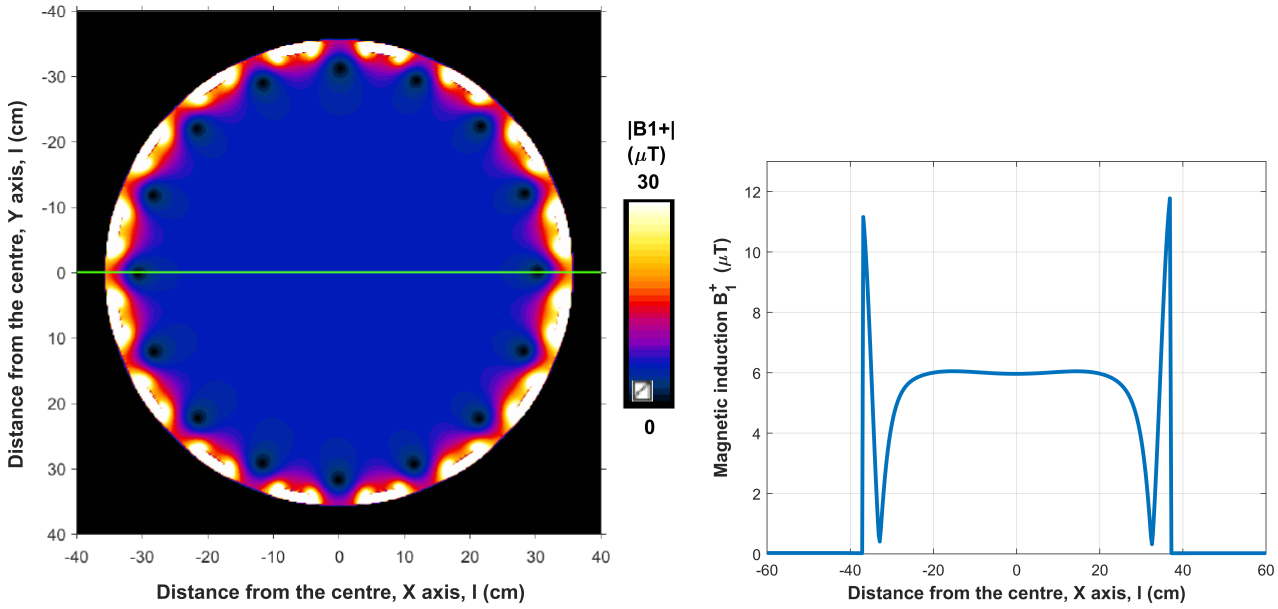

(A). B_1^+ field where the green line shows the location of the slice.

(B). B_1^+ field in slice.

Figure 4. Homogeneous B_1^+ field of an empty tuned coil.

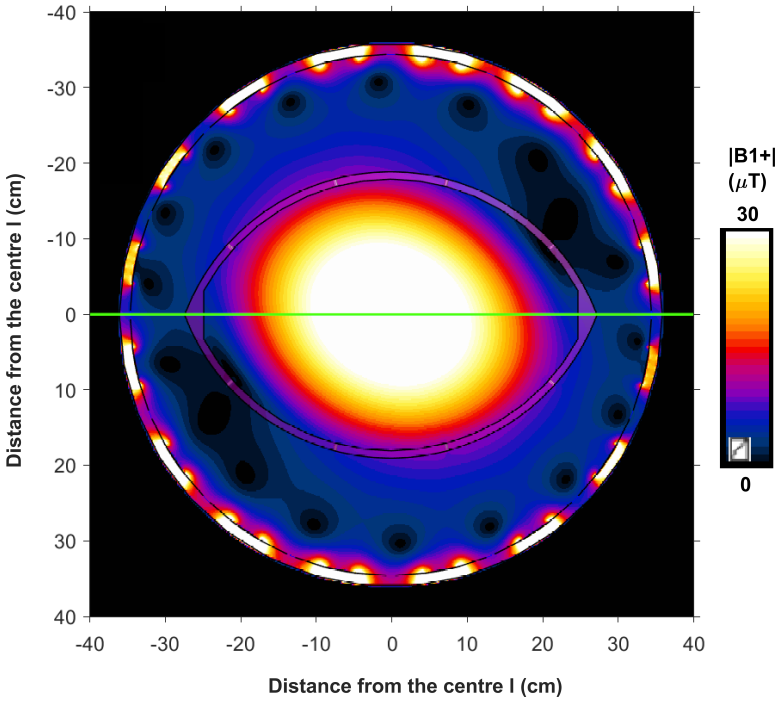

Figure 5. Change in B_1^+ field homogeneity due to the Sigma-Eye applicator model.

shows the temperature increase for MR exposure using a 700 W turned on for two second (20 seconds scanning and 10 % duty cycle) every ten minutes was added to the simulated HT treatment. Table 2 contains information about the temperature increase caused by RF MR exposure.

4. Discussion

On average, the predicted temperature during the regional HT was increased by 0.027 °C, when adding RF exposure during the non-invasive MR temperature measurements to the regional HT. This temperature increase is below the required clinical resolution for temperature monitoring probes of 0.1 °C, and thus in HT, the temperature range of 40–44 °C can be considered insignificant [25]. The temperature increase occurs only during the application of the RF MR excitation every ten minutes and after its termination, the temperature always slowly decreases to the values of the simulated HT treatment. In comparison with the study done by Shellock et al. [26], the values of the temperature gradient correspond to those obtained from the former MR scans. However,

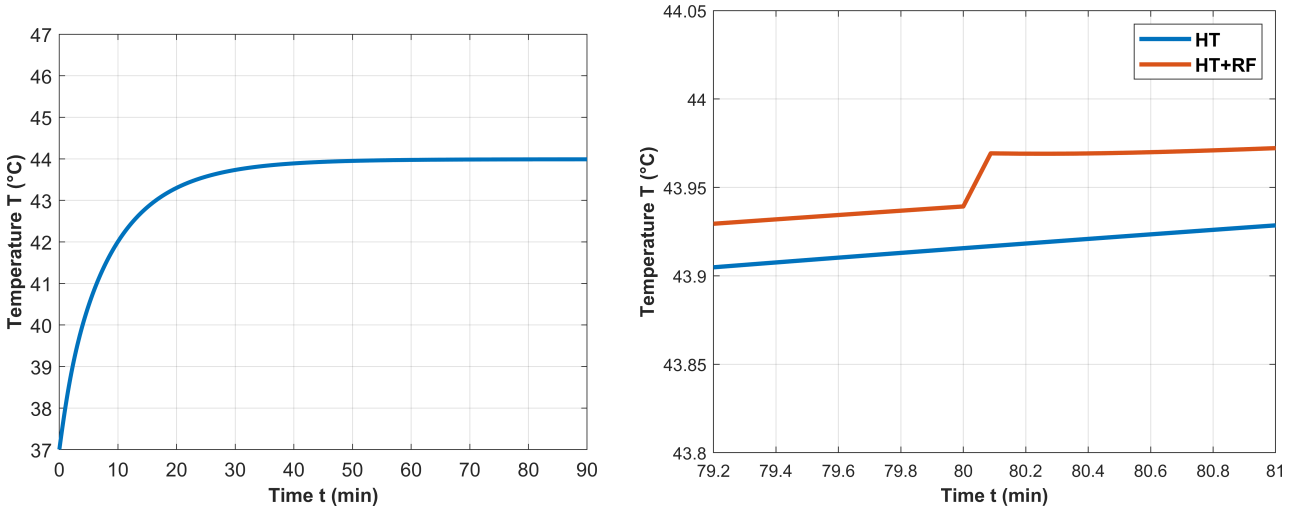

(A). Temperature increase throughout the 90-minute HT treatment at the point of the 44 °C increase.

(B). Detail of the temperature increase caused by adding the RF MR exposure to the HT treatment.

FIGURE 6. Example of predicted temperature profile during the deep regional HT treatment.

Patient model	$\lvert B_1^+ \rvert$ **[µT]**	**psSAR 10 g [W kg^{-1}]**	ΔT **[°C]**
CT model	10.57 ± 0.95	77.36	0.03
Duke	9.94 ± 0.41	70.10	0.02
Ella	12.91 ± 1.36	117.20	0.03

TABLE 2. RF MRI exposure temperature elevation in contrast with obtained magnetic field homogeneity distortion and peak-spatial 10 g SAR parameter (psSAR) calculated for 700 W.

the RF exposure during MR thermometry scanning is lower in comparison to the standard scanning due to the fact the MR thermometry is done every ten minutes.

The deep regional HT uses constructive interference of several EM waves radiated from individual antenna elements in the phased array setup to calculate the specific absorption rate distribution and temperature map. Given the potential variations in local SAR due to increased B_1^+ field intensity, we also assessed the impact of the HT applicator and patient models on the B_1^+ field homogeneity. The homogeneity of the B_1^+ field depends on the object size placed inside the MR coil and its dielectric properties. According to our simulations, the HT applicator water bolus has increased the magnitude of the B_1^+ field by factor of a 4.75, in comparison to the scenario of an empty reference coil. This indicate that a lower input power of the birdcage coil is necessary during the HT MR scans to obtain an identical flip angle within the patient. The limiting factor is that the objects placed in the birdcage coil itself have certain capacitive properties, and therefore a slight shift in the coil resonant frequency may occur.

Sigma Eye along with BSD-2000 3D MR applicator (Pyrexar Medical, Salt Lake City, USA), both consisting of 12 dipole antenna pairs, are currently the only clinical phased array systems compatible with the MR scanner for hyperthermia treatment in the pelvic region [27]. Other possible elements, such as waveguides, patch, or metamaterial antennas, are too robust to fit into an MR scanner, or contain large metallic structures that might result in creation of an eddy currents [28–31]. In addition, due to the necessity of small FDTD discretisation step of the Sigma Eye model and available computation resources, we did not include Faraday cage in our model. We applied the UPML boundary conditions in a distance of 500 mm from the birdcage coil, which we assume did not influenced temperature predictions in the human models placed within the MR bore.

5. CONCLUSION

This in-silico study shows the insignificant impact of MR thermometry on the predicted temperature during a regional hyperthermia treatment in the pelvic region using Sigma Eye applicator. Our findings demonstrate the minimal impact of the RF exposure on the temperature increase, confirming the reliability of this 3D noninvasive temperature monitoring method during the regional hyperthermia.

ACKNOWLEDGEMENTS

This study was supported by the Student Grant Competition of CTU, grants No. SGS24/112/OHK4/2T/17 and SGS23/199/OHK4/3T/17. The authors would like to thank Zürich MedTech AG (`https://www.zmt.swiss`), for providing the Sim4Life for Science license, enabling this research.

REFERENCES

[1] J. Van der Zee. Heating the patient: A promising approach? *Annals of Oncology* **13**(8):1173–1184, 2002. `https://doi.org/10.1093/annonc/mdf280`

[2] R. D. Issels, L. H. Lindner, J. Verweij, et al. Effect of neoadjuvant chemotherapy plus regional hyperthermia on long-term outcomes among patients with localized high-risk soft tissue sarcoma: The EORTC 62961-ESHO 95 randomized clinical trial. *JAMA Oncology* **4**(4):483–492, 2018. https://doi.org/10.1001/jamaoncol.2017.4996

[3] N. R. Datta, E. Stutz, S. Gomez, S. Bodis. Efficacy and safety evaluation of the various therapeutic options in locally advanced cervix cancer: A systematic review and network meta-analysis of randomized clinical trials. *International Journal of Radiation Oncology, Biology, Physics* **103**(2):411–437, 2019. https://doi.org/10.1016/j.ijrobp.2018.09.037

[4] H. P. Kok, J. Crezee. Validation and practical use of Plan2Heat hyperthermia treatment planning for capacitive heating. *International Journal of Hyperthermia* **39**(1):952–966, 2022. https://doi.org/10.1080/02656736.2022.2093996

[5] A. Bakker, R. Zweije, H. P. Kok, et al. Comparison of the clinical performance of a hybrid Alba 4D and the AMC-4 locoregional hyperthermia systems. *International Journal of Hyperthermia* **39**(1):1408–1414, 2022. https://doi.org/10.1080/02656736.2022.2140841

[6] H. P. Kok, G. C. van Rhoon, T. D. Herrera, et al. Biological modeling in thermoradiotherapy: present status and ongoing developments toward routine clinical use. *International Journal of Hyperthermia* **39**(1):1126–1140, 2022. https://doi.org/10.1080/02656736.2022.2113826

[7] I. VilasBoas-Ribeiro, M. Franckena, G. C. van Rhoon, et al. Using MRI to measure position and anatomy changes and assess their impact on the accuracy of hyperthermia treatment planning for cervical cancer. *International Journal of Hyperthermia* **40**(1):2151648, 2023. https://doi.org/10.1080/02656736.2022.2151648

[8] H. P. Kok, P. M. A. van Haaren, J. B. van de Kamer, et al. High-resolution temperature-based optimization for hyperthermia treatment planning. *Physics in Medicine & Biology* **50**(13):3127, 2005. https://doi.org/10.1088/0031-9155/50/13/011

[9] J. Gellermann, J. Göke, R. Figiel, et al. Simulation of different applicator positions for treatment of a presacral tumour. *International Journal of Hyperthermia* **23**(1):37–47, 2007. https://doi.org/10.1080/02656730601121549

[10] T. Drizdal, M. Novak. Application of an artificial intelligence segmentation for deep hyperthermia treatment planning in the pelvic region. *Acta Polytechnica* **63**(6):383–389, 2023. https://doi.org/10.14311/AP.2023.63.0383

[11] H. P. Kok, J. Crezee. Adapt2Heat: Treatment planning-assisted locoregional hyperthermia by on-line visualization, optimization and re-optimization of SAR and temperature distributions. *International Journal of Hyperthermia* **39**(1):265–277, 2022. https://doi.org/10.1080/02656736.2022.2032845

[12] H. P. Kok, J. Crezee. Hyperthermia treatment planning: Clinical application and ongoing developments. *IEEE Journal of Electromagnetics, RF and Microwaves in Medicine and Biology* **5**(3):214–222, 2021. https://doi.org/10.1109/jerm.2020.3032838

[13] A. Bakker, R. Zweije, G. van Tienhoven, et al. Two high-resolution thermal monitoring sheets for clinical superficial hyperthermia. *Physics in Medicine & Biology* **65**(17):175021, 2020. https://doi.org/10.1088/1361-6560/ab9bc2

[14] F. Lestini, N. Panunzio, G. Marrocco, C. Occhiuzzi. Epidermal RFID-based thermal monitoring sheet (R-TMS) for microwave hyperthermia. *IEEE Journal of Electromagnetics, RF and Microwaves in Medicine and Biology* **7**(4):365–374, 2023. https://doi.org/10.1109/JERM.2023.3299525

[15] T. V. Feddersen, D. H. J. Poot, M. M. Paulides, et al. Multi-echo gradient echo pulse sequences: Which is best for PRFS MR thermometry guided hyperthermia? *International Journal of Hyperthermia* **40**(1):2184399, 2023. https://doi.org/10.1080/02656736.2023.2184399

[16] T. V. Feddersen, J. A. Hernandez-Tamames, M. M. Paulides, et al. Magnetic resonance thermometry for hyperthermia in the oropharynx region. *International Journal of Hyperthermia* **41**(1):2352545, 2024. https://doi.org/10.1080/02656736.2024.2352545

[17] H. Odéen, D. L. Parker. Magnetic resonance thermometry and its biological applications–physical principles and practical considerations. *Progress in Nuclear Magnetic Resonance Spectroscopy* **110**:34–61, 2019. https://doi.org/10.1016/j.pnmrs.2019.01.003

[18] J. Blackwell, M. J. Kraśny, A. O'Brien, et al. Proton resonance frequency shift thermometry: A review of modern clinical practices. *Journal of Magnetic Resonance Imaging* **55**(2):389–403, 2022. https://doi.org/10.1002/jmri.27446

[19] T. Drizdal, M. R. Tarasek, R. Pellicer, et al. Influence of deep-region RF hyperthermia system on B1+ field of 1.5 T MR scanner: A simulation study. In *Proceedings of International Socciety for Magnetic Resonance in Medicine*, vol. 22, p. 1364. International Socciety for Magnetic Resonance in Medicine, 2014.

[20] J. Chi, F. Liu, E. Weber, et al. GPU-accelerated FDTD modeling of radio-frequency field–tissue interactions in high-field MRI. *IEEE Transactions on Biomedical Engineering* **58**(6):1789–1796, 2011. https://doi.org/10.1109/TBME.2011.2116020

[21] M. Murbach, E. Neufeld, M. Capstick, et al. Thermal tissue damage model analyzed for different whole-body SAR and scan durations for standard MR body coils. *Magnetic Resonance in Medicine* **71**(1):421–431, 2014. https://doi.org/10.1002/mrm.24671

[22] P. Wust, H. Fähling, W. Wlodarczyk, et al. Antenna arrays in the SIGMA-eye applicator: interactions and transforming networks. *Medical Physics* **28**(8):1793–1805, 2001. https://doi.org/10.1118/1.1388220

[23] M.-C. Gosselin, E. Neufeld, H. Moser, et al. Development of a new generation of high-resolution anatomical models for medical device evaluation: The Virtual Population 3.0. *Physics in Medicine & Biology* **59**(18):5287, 2014. https://doi.org/10.1088/0031-9155/59/18/5287

[24] A. Christ, W. Kainz, E. G. Hahn, et al. The Virtual Family – development of surface-based anatomical models of two adults and two children for dosimetric simulations. *Physics in Medicine & Biology* **55**(2):N23, 2010. https://doi.org/10.1088/0031-9155/55/2/N01

[25] H. D. Trefná, H. Crezee, M. Schmidt, et al. Quality assurance guidelines for superficial hyperthermia clinical trials: I. Clinical requirements. *International Journal of Hyperthermia* **33**(4):471–482, 2017. https://doi.org/10.1080/02656736.2016.1277791

[26] F. G. Shellock, D. J. Schaefer, J. V. Crues. Alterations in body and skin temperatures caused by magnetic resonance imaging: Is the recommended exposure for radiofrequency radiation too conservative? *British Journal of Radiology* **62**(742):904–909, 1989. https://doi.org/10.1259/0007-1285-62-742-904

[27] S. Curto, H. T. Mulder, B. Aklan, et al. A multi-institution study: Comparison of the heating patterns of five different MR-guided deep hyperthermia systems using an anthropomorphic phantom. *International Journal of Hyperthermia* **37**(1):1103–1115, 2020. https://doi.org/10.1080/02656736.2020.1810331

[28] O. Fišer, I. Merunka, J. Vrba. Waveguide applicator system for head and neck hyperthermia treatment. *Journal of Electrical Engineering and Technology* **11**(6):1744–1753, 2016. https://doi.org/10.5370/JEET.2016.11.6.1744

[29] D. Vrba, J. Vrba, D. B. Rodrigues, P. Stauffer. Numerical investigation of novel microwave applicators based on zero-order mode resonance for hyperthermia treatment of cancer. *Journal of the Franklin Institute* **354**(18):8734–8746, 2017. https://doi.org/10.1016/j.jfranklin.2016.10.044

[30] J. Crezee, R. Zweije, J. Sijbrands, H. P. Kok. Dedicated 70 MHz RF systems for hyperthermia of challenging tumor locations. *International Journal of Microwave and Wireless Technologies* **12**(9):839–847, 2020. https://doi.org/10.1017/S1759078720000318

[31] M. R. S. Ramu, K. Arunachalam. Miniaturized 434 MHz cavity encapsulated patch antenna for superficial hyperthermia treatment. *IEEE Journal of Electromagnetics, RF and Microwaves in Medicine and Biology* **7**(4):392–399, 2023. https://doi.org/10.1109/JERM.2023.3307220